Hindawi
International Journal of Corrosion
Volume 2021, Article ID 6666811, 15 pages
https://doi.org/10.1155/2021/6666811

Research Article

Investigation of Corrosion Protection of Austenitic Stainless Steel in 5.5 M Polluted Phosphoric Acid Using 5-Azidomethyl-7-morpholinomethyl-8-hydroxyquinoline as an Ecofriendly Inhibitor

Aimad Mazkour,[1] Souad El Hajjaji,[1] Najoua Labjar,[2] El Mostapha Lotfi,[2] and Mohammed El Mahi[2]

[1]*Laboratory of Spectroscopy, Molecular Modeling, Materials, Nanomaterials, Water and Environment, CERN2D, Faculty of Sciences, Mohammed V University in Rabat, Rabat, Morocco*
[2]*Laboratory of Spectroscopy, Molecular Modeling, Materials, Nanomaterials, Water and Environment, CERN2D, ENSAM, Mohammed V University in Rabat, Rabat, Morocco*

Correspondence should be addressed to Souad El Hajjaji; selhajjaji@hotmail.com

Received 7 November 2020; Revised 30 March 2021; Accepted 19 April 2021; Published 15 May 2021

Academic Editor: Michael J. Schütze

The use of 5-azidomethyl-7-morpholinomethyl-8-hydroxyquinoline (AMH) as a corrosion inhibitor for AISI 321 stainless steel in 5.5 M polluted phosphoric acid was investigated using the hydrogen evolution technique, linear polarization curves, and impedance spectroscopy. Impedance measurements revealed that the dissolution of AISI 321 in 5.5 M polluted phosphoric acid was controlled by an activation mechanism, unchanged even with the addition of AMH at different concentrations. Polarization results showed that the inhibition ability was enhanced with increasing inhibitor concentration. AMH acted as a mixed-type inhibitor by random adsorption on the alloy surface, whatever the nature of the reaction that is taking place. The adsorption of AMH on the AISI 321 surface was also discussed via the Langmuir adsorption isotherm. The influence of elevating the solution temperature on the corrosion inhibition performance was studied. A quantum chemistry study with the DFT method was also conducted, which supplied a logical and exploitable theoretical explanation of the adsorption and the inhibition action of AMH on AISI 321.

1. Introduction

The different properties of stainless steels, namely, the mechanical strength and the corrosion resistance even in very aggressive environments, make them very commonly used in the phosphoric acid manufacturing plants. The oxide layer appearing on the surface of stainless steels in contact with air and/or water represents a barrier that protects these materials against undesirable and destructive reactions in surrounding environments [1]. Generally, the corrosion resistance of stainless steel depends mainly on the stability of the oxide film grown on its surface. However, the oxide film or passive film can be altered by the severe working conditions (high acidity, high temperature…) and the presence of impurities in the industrial acids. In fact, most of the world's phosphoric acid production is manufactured by wet process, which consists in reacting natural phosphate with a solution of sulfuric acid followed by a filtration. This technique produces a phosphoric acid containing several impurities (halogen, sulphates, gypsum particles…) that can break the passive film protection and seriously damage these materials [2]. To overcome this problem, the use of inhibitors is an effective and original method against corrosion phenomenon. In addition, the use of inhibitors for commonly used stainless steels spares the industry the economic burden of using materials with high levels of alloying elements that are too expensive. Inhibitors for corrosion protection are substances that slow down or stop the corrosion process

following their adsorption on the metal surface. Generally, the ability of a substance to inhibit metal corrosion depends essentially on the presence of heteroatoms (O, N, S…), its structure, its electronic properties, the aromaticity, and the nature of π orbital donor electrons [3]. Furthermore, as guidelines for the use of inhibitors become more stringent and exigent on the ecological aspect, the development of biodegradable and environmentally compatible or ecofriendly inhibitors is becoming an important issue [4]. Many studies were focused on the corrosion inhibition of stainless steels in acidic environments, but there are few researches regarding concentrated and polluted phosphoric acid as an aggressive medium [5, 6]. The 8-hydroxyquinoline molecule and its derivatives are widely used ligands because of their various effects related to their complexing character towards metal ions. The treatment of aqueous solutions containing heavy metals and the selective extraction of strategic metals from their ores and the development of products for pharmacological activities remain possible domains for the use of these substances [7–9]. 5-Azidomethyl-7-morpholinomethyl-8-hydroxyquinoline is one of 8-hydroxyquinoline derivatives, obtained by Mannich reaction with high extraction efficiency and which has revealed important antioxidant properties [10].

The aim of the present study was to investigate the inhibition ability of 5-azidomethyl-7-morpholinomethyl-8-hydroxyquinoline on the corrosion of AISI 321 stainless steel in 5.5 M polluted phosphoric acid medium, using the hydrogen evolution technique, polarization curves, and impedance spectroscopy. Quantum chemical calculations were also performed to define the electronic structure and the energetic state of the molecule as well as the relationship between the theoretical data and the inhibition behaviour.

2. Materials and Methods

2.1. Material and Test Solution. The material tested in the present study was a commercial AISI 321 austenitic stainless steel. This material is commonly used in several industries including petroleum, oil, medicine, and electrochemical industries because of their strength, high quality, good resistance, weldability, mechanical properties, and relatively low cost [11]. The weight percentages of AISI 321 alloying elements obtained by spectroscopic analysis are given in Table 1.

Figure 1 illustrates an image by optical microscopy of the AISI 321 surface as received, showing the presence of single-phase grains of austenite. The used AISI 321 specimens had a cylindrical form with an exposure area of 1 cm^2. The specimens were subjected to a mechanical treatment that consists of polishing with sandpaper of different particle sizes (120, 240, 600, 1200, 1500, and 2000). The samples were then ultrasonically degreased and degassed in acetone, rinsed with double distilled water, and dried with a hot air blower before being mounted in the electrochemical cell.

In order to simulate the degrading conditions of this material within the phosphoric acid manufacturing plant, a polluted phosphoric acid was used at different temperatures. This solution consists of a commercial acid with a concentration of 5.5 M similar to that of the industrial phosphoric acid (the solution pH was 0.62); to which are added certain impurities that proved negative effects in the corrosion process of stainless steels in industrial phosphoric acid. The concentrations of these impurities were 2 wt.% and 0.06 wt.% for H_2SO_4 and KCl, respectively [12]. The name of the polluted phosphoric acid will be attributed to this solution in all of this paper.

2.2. The Inhibitor Molecule. The molecules derived from 8-hydroxyquinoline are among the most interesting quinoline heterocycles, which have undergone a very remarkable and rapid development in the last few years. These chelating agents solve many problems of analysis, because of their high efficiency in extraction and their pharmacological and biological activities [7–9]. In this study, 5-azidomethyl-7-morpholinomethyl-8-hydroxyquinoline (AMH), a derivative of 8-hydroxyquinoline, was used as an inhibitor of AISI 321 in 5.5 M polluted phosphoric acid. The chemical structure of this molecule is given in Figure 2. The used AMH concentrations varied from 0.5 to 5 mmol/L, and the polluted phosphoric acid solution in the absence of AMH was taken as blank for comparison.

2.3. Hydrogen Evolution Technique. The measurement of the hydrogen released during the corrosion process is considered as a simple and reliable method to investigate the protective performance of an inhibitor in acidic environments. The conventional method of weight loss has certain disadvantages that sometimes make it difficult to interpret the results, especially when dealing with passivating materials. The measurements of the hydrogen evolution rate were carried out at 20°C using the simple assembly illustrated in Figure 3.

The stainless steel sample was placed in an Erlenmeyer containing the aggressive solution. A pipe was used to connect the Erlenmeyer with an inverted graduated cylinder, mounted over a trough. The cylinder is initially filled with the aggressive solution. Hydrogen released from the sample entered the cylinder and progressively displaced the solution. Thus, the volume of hydrogen evolved was easily measured by reading the position of the solution level in the graduated cylinder [13].

The inhibitor efficiency is directly calculated from the volume of hydrogen released by the following relation:

$$\%IE = \frac{V_0 - V_i}{V_0} \times 100, \quad (1)$$

where V_0 and V_i are the hydrogen gas evolved in the absence and the presence of the inhibitor, respectively.

2.4. Electrochemical Measurements. All the electrochemical tests, namely, E_{ocp} vs time, polarization curves, and impedance spectroscopy, were realized with electrochemical equipment involving three kinds of electrodes: a platinum auxiliary electrode, a second kind electrode (Cl | Hg_2Cl_2 (calomel) | Hg| Pt) as reference electrode, and AISI 321 as a working electrode. The measurements were carried out using a BioLogic SP 150 potentiostat galvanostat, controlled by EC-Lab V11.01 analysis software. The mechanical pretreatment of samples proved insufficient to remove the oxide layer previously

Table 1: Elemental composition of as-received AISI 321 stainless steel (wt.%).

Cr	Ni	C	Si	Mn	Ti	S	Mo	Cu	Nb	Fe
19.1	9.85	0.086	0.297	1.65	0.68	0.05	0.16	0.172	0.035	Remainder

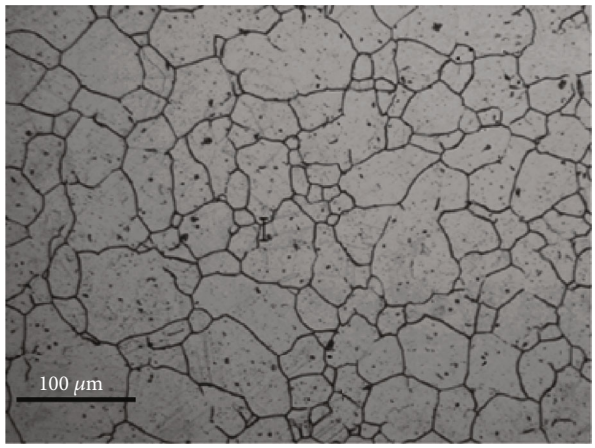

Figure 1: Optical micrograph of as-received AISI 321 stainless steel.

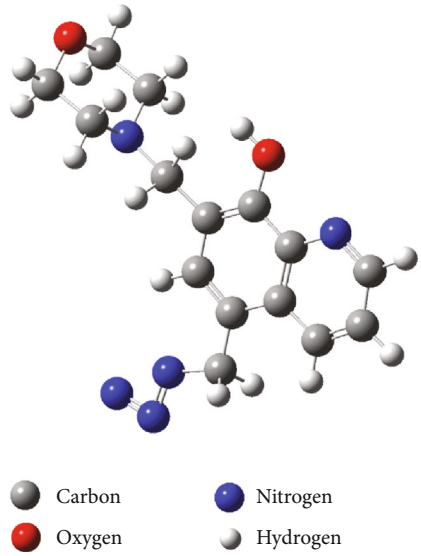

Figure 2: Molecular structure of 5-azidomethyl-7-morpholinomethyl-8-hydroxyquinoline.

formed on the surface. Therefore, the potential of −1 V/SCE was applied for 15 min before starting any electrochemical test. The electrochemical behaviour of the AISI 321 sample in inhibited and uninhibited solution was studied by recording anodic and cathodic polarization curves. The potential applied to the specimen varies gradually from −0.8 V/SCE to 1.2 V/SCE with a sweeping rate of 50 mV·min^{-1}. Polarization data was treated using EC-Lab V11.01 software, and Tafel extrapolation method was followed to obtain corrosion current density values. The inhibition efficiency was calculated from the measured I_{corr} values using the following relation:

$$\%IE = \left(\frac{I^{o}_{corr} - I^{i}_{corr}}{I^{o}_{corr}}\right) \times 100, \quad (2)$$

where I^{o}_{corr} and I^{i}_{corr} are uninhibited and inhibited corrosion current densities, respectively.

The electrochemical impedance spectroscopy (EIS) measurements were carried out after 60 minutes of immersion at the abandon potential in a solution open to the atmosphere. The sinusoidal wave voltage is 10 mV peak to peak at frequencies between 10^{5} and 10^{-2} Hz. The impedance diagrams are provided in Bode and Nyquist representations. The impedance curve fitting was carried out by the EC-Lab V11.01 software. Each experiment was repeated three times to check reproducibility. The inhibition efficiency was calculated from the charge transfer resistance values using the following equation:

$$\%IE = \left(1 - \frac{R^{\circ}_{ct}}{R_{ct}}\right) \times 100, \quad (3)$$

where R°_{ct} and R_{ct} are the charge transfer resistance in the absence and in the presence of the inhibitor, respectively.

2.5. Quantum Chemical Study. 5-Azidomethyl-7-morpholinomethyl-8-hydroxyquinoline (AMH) was sketched using the GaussView 5.0 program, and Gaussian 09W software was employed in quantum calculations after geometry optimization. AMH electronic properties were investigated by density functional theory (DFT) using B3LYP hybrid functional with a 6-31G∗ basis set. This approach was chosen because of its high accuracy and reliability. It requires less computation time and provides identical precision for medium and large organic molecules. The solvent effect was taken into consideration in the calculations. The estimated theoretical quantum parameters were molecular energy (E), the energy of the lowest unoccupied molecular orbital (E_{LUMO}), the energy of the highest occupied molecular orbital (E_{HOMO}), energy band gap (ΔE), and dipole moment (μ). Additional parameters, namely, chemical hardness (η), electronegativity (χ), and fraction of electron transferred (ΔN), are also calculated using the following relations:

$$\eta = -\frac{1}{2}(E_{HOMO} - E_{LUMO}),$$
$$\chi = \frac{(-E_{HOMO} - E_{LUMO})}{2}, \quad (4)$$
$$\Delta N = \frac{\chi_{Fe} - \chi_{inh}}{2(\eta_{Fe} - \eta_{inh})},$$

where χ_{Fe} is the iron electronegativity (=7 eV) and η_{Fe} is the iron hardness (=0), assuming that the parameters of stainless steel are similar to those of iron since AISI 321 contains more than 65% of iron.

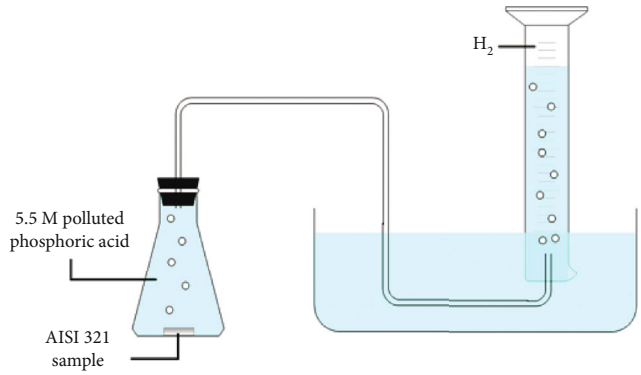

Figure 3: Illustration of the setup for measuring the volume of hydrogen released.

3. Results and Discussion

3.1. Hydrogen Evolution. For metal corrosion in acidic environments, the amounts of H_2 released by the cathodic reaction are proportional to the corroded amounts of metal. Therefore, measuring the hydrogen-collected gas on the metal surface over time can provide valuable information on the corrosion process. The effect of increasing concentration of AMH on the corrosion inhibition of AISI 321 dipped in 5.5 M polluted phosphoric acid is evaluated by recording the evolution of hydrogen gas released for 48 hours. The results are shown in Figure 4. In order to guarantee the reproducibility of the results, the experiences were executed three times and the results presented below report an average of the tests.

It is obvious that the volume of hydrogen released grows almost linearly with the time of exposure for all cases. It should be noted that the corrosion rate could be determined from the slopes of such curves, which implies that the corrosion rate is not significantly changed over time. AISI 321 specimens without AMH exhibited highest H_2 released values throughout the test. The addition of different concentrations of AMH causes a gradual lowering in the H_2 released, i.e., a decrease in the corrosion rate of AISI 321. This behaviour can be justified by the rise in the concentration of AMH that causes an increase in the surface of AISI 321 wrapped by the inhibitor [13]. Inhibition efficiency grows with elevating AMH concentration and reaches a maximum value of about 97.4% for a concentration of 5 mmol/L. The corresponding efficiencies increase slightly over time, which may be the result of a displacement of the adsorption-desorption equilibrium in the forward direction and/or the growth of an oxide film on AISI 321 surface which becomes more stable and protective with the exposure time. AISI 321 oxidation in 5.5 M polluted phosphoric acid is suggested as a general corrosion characterized by a loss of thickness easily detectable by a simple observation of the surface by the naked eye (Figure 5). Furthermore, an anodic cyclic potentiodynamic polarization of AISI 321 in 5.5 M polluted phosphoric acid at 20°C after one hour of immersion time was registered (Figure 5) and shows a superposition of the forward and backward lines of the curve, indicating the absence of any stable pitting on the surface [14]. In that case, the results of the hydrogen released allow quantifying the damage (thickness loss per unit of time), by using the following relation:

$$V_{\text{corr}} = \frac{\Delta V_{\text{H2}} \times M}{V_{\text{mol}} \times \rho}, \tag{5}$$

where V_{corr} is the corrosion rate (cm/year), ΔV_{H2} is H_2 released per units of surface and time ($\text{L}\cdot\text{cm}^{-2}\cdot\text{year}^{-1}$), V_{mol} is the molar volume (24.055 $\text{L}\cdot\text{mol}^{-1}$ at 20°C under an atmosphere), M is the molar mass of stainless steel (g/mol), and ρ is the alloy density (g/cm^3).

The results of thickness loss values of AISI 321 in 5.5 M polluted phosphoric acid without and with the addition of various concentrations of AMH and the corresponding efficiencies, deduced from hydrogen evolution tests, are shown in Table 2. The relatively large value of AISI 321 thickness loss of continuous contact with the polluted phosphoric acid reveals that it is nonresistant to this medium. The addition of different concentrations of AMH has improved corrosion resistance by adsorbing to the surface and thus reducing the corrosion rate. The loss in thickness of AISI 321 decreases and reached a minimum value of 0.05 mm/year for a concentration of 5 mmol/L, which corresponds to an efficiency of 97.6%. Consequently, the use of this alloy becomes comparable to the use of special stainless steels with high alloying elements [12].

These results confirm that AMH effectively prevents the corrosion of AISI 321. This method has the advantage of being a simple execution, not requiring an important set-up, but provides no additional information regarding the mechanisms implied in the corrosion process.

3.2. Open Circuit Potential (OCP) and Tafel Polarization Measurements. The open circuit potential represents the measured voltage when no current is flowing in the cell. Recording this potential over time can provide valuable information about the state of the metal surface and the changes that can occur on it. Moreover, the validity of some methods such as impedance is based on the stability of the OCP potential. Figure 6 represents the evolution of the OCP of AISI 321 versus time in 5.5 M polluted phosphoric acid solution in the absence and in the presence of various concentrations of AMH at 20°C.

In all cases, the OCP value varies towards less negative potentials over time. The formation of an oxide film on the AISI 321 surface and its growth following its interaction with the phosphoric acid solution induced an enhancement of the OCP value [15]. Because the important level of chromium (19.1%) that can ensure the development of a stable oxide layer on the AISI 321 surface, surface oxide development proceeds until a stable thickness is achieved in the surrounding medium [12]. It can be easily seen that the presence of AMH displaces the OCP towards more anodic values for all the studied concentrations. The maximum-recorded interval between OCP potentials without and with the addition of different concentrations of AMH is approximately 19 mV for the concentration of 5 mmol/L. Following the hypothesis of Pradityana et al. [16], this may indicate that AMH acts as a

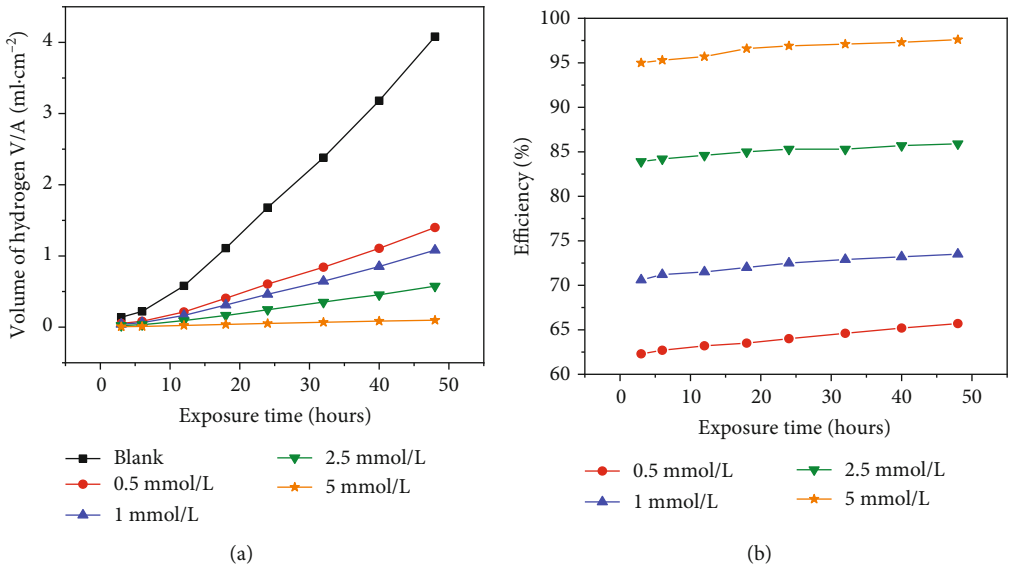

Figure 4: Evolution of hydrogen gas released (a) and the corresponding inhibition efficiencies (b) over time for AISI 321 in 5.5 M polluted phosphoric acid in the absence and in the presence of different concentrations of AMH at 20°C.

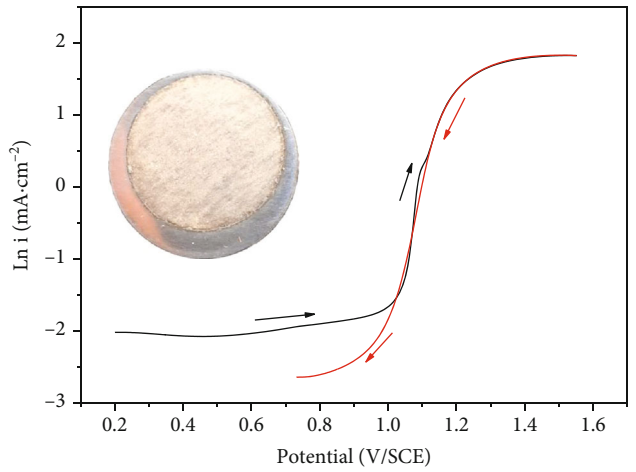

Figure 5: Anodic cyclic potentiodynamic polarization of AISI 321 in 5.5 M polluted phosphoric acid at 20°C after 1 hour of immersion and a general view of the surface state. Arrows indicate the direction of the scan.

Table 2: Thickness loss values and corresponding efficiencies deduced from hydrogen evolution tests.

Inhibitor concentration (mmol/L)	Thickness loss (mm/year)	Efficiency (%)
Blank	2.2	—
0.5	0.75	65.7
1	0.58	73.5
2.5	0.31	85.9
5	0.05	97.6

mixed-type inhibitor since this difference does not exceed 85 mV. The positive OCP shift in the presence of the inhibitor suggests that AMH can inhibit AISI 321 corrosion which mostly controls the anodic process. However, there was not a direct and evident link between the steady-state potential and the concentration of AMH.

In order to determine the anodic and cathodic mechanisms and kinetics of AISI 321 corrosion and their modifications by the addition of the inhibitor, the samples were polarized cathodically and anodically to plot potentiodynamic polarization curves. The current-potential relationships for AISI 321 in 5.5 M polluted phosphoric acid with different concentrations of AMH are given in Figure 7. The electrochemical parameters extracted from the polarization curves, including mixed potential (E_{cor}), corrosion current density (I_{cor}), critical current density (I_{crit}), passivation current density (I_{pas}), and inhibition efficiency (E%) are gathered in Table 3. It should be noted that the occurrence of the active-passive transition on the anodic zone of such curves restricts the potential interval for the linear behaviour of Tafel, which makes it difficult to accurately specify the corresponding Tafel tangent. However, according to other authors [17, 18], the extrapolation of the cathodic reduction must be sufficient to determine the corrosion current density by extrapolation of Tafel to the abandon potential. This oncoming would provide the net value of the cathodic process rate to the abandon potential. It is as well as the net value of the anodic reaction rate to the abandon potential that has been checked by other nonelectrochemical methods [19].

In all cases, potentiodynamic polarization curves exhibit the same general form with a large passivity interval characterized by a low and negligible dependence between current density and the applied potential as shown in Figure 7.

The potentiodynamic polarization results indicate that the presence of AMH diminishes the anodic dissolution

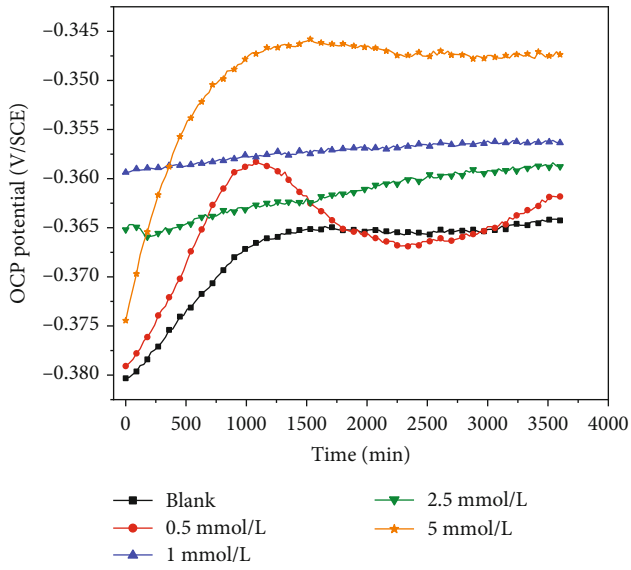

Figure 6: The open circuit potential (OCP) of experimental AISI 321 in 5.5 M polluted phosphoric acid without and with various concentrations of AMH around 20°C.

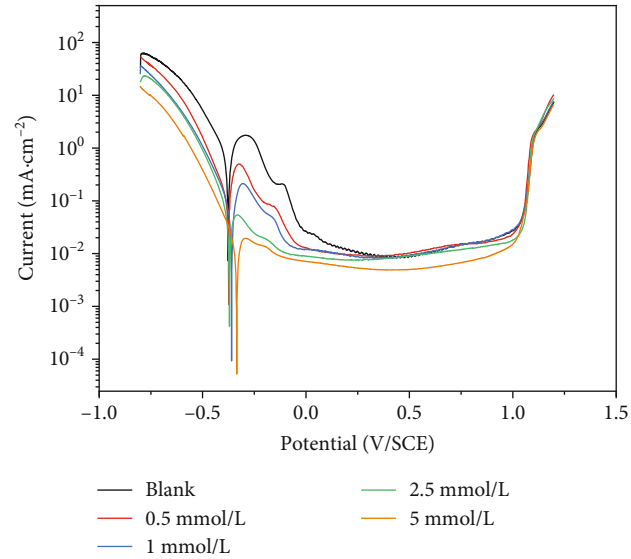

Figure 7: Polarization curves of AISI 321 in 5.5 M polluted phosphoric acid containing various concentrations of AMH at 20°C.

and reduces the hydrogen reduction on the cathodic location of AISI 321. The cathodic curves exponentially progress to Tafel lines suggesting that the hydrogen reduction at the AISI 321 surface occurs by a pure activation mechanism. The addition of AMH does not greatly change the Tafel slope value, which means that adding the inhibitor has almost no influence on the proton reduction mechanism. This fact reinforces the consideration of the direct relationship between the current diminution and the area covered by the inhibitor and in particular when describing the adsorption of the AMH and its nonreactive blocking of the metal surface. Whatever the concentration of AMH added to the aggressive solution, neither the primary passive potential (E_{pp}) nor the transpassive potential (E_{trans}) of AISI 321 was affected. Nevertheless, the corresponding critical current (i_{crt}) progressively reduced with the rise of AMH concentration. i_{crt} is the maximum active peak current density of AISI 321 after which a removal occurs due to the development of an oxide film at the alloy surface. The presence of the inhibitor was found to reduce critical current, thus supporting the formation of an oxide film, which resulted in a more stable oxide range and lower dissolution of the oxide as shown in Figure 7 [13, 20]. All these results indicate that AMH plays the role of a mixed inhibitor for AISI 321 in 5.5 M polluted phosphoric acid. The data presented in Table 3 show that increasing AMH concentration decreases the corrosion current density (I_{corr}) and increases the inhibition efficiency, with a shift in the corrosion potential to more anodic values. Inhibition efficiency increases with AMH concentration to attain a maximum value of 95.57% for 5 mmol/L of the inhibitor.

3.3. Electrochemical Impedance Spectroscopy Analysis (EIS). To define the changes induced by the addition of AMH at the interface AISI 321/5.5 M H_3PO_4 and to investigate the stability of the passive film formed on the AISI 321 surface, an impedance analysis was conducted. Nyquist and Bode plots of AISI 321 were recorded under potentiostatic conditions after one hour of immersion in 5.5 M polluted phosphoric acid in the absence and in the presence of AMH. The results are illustrated in Figure 8.

The Nyquist curves have almost the same shape for all AMH concentrations, indicating that the corrosion mechanism is not changed by the addition of the inhibitor as shown in polarization curves. These diagrams show single imperfect and depressed semicircles over the frequency range, meaning that the metal oxidation is controlled by a charge-transfer reaction [13, 21]. A significant increase in capacitive half-loop size is observed with the rise of AMH concentration, indicating that the inhibition efficiency is a function of the concentration of the inhibitor, and this may be related to the adsorption and the reinforcement of the inhibiting film on the AISI 321 surface. In the Bode representation, all curves are less than 90°. This implies that the use of a constant phase element (CPE) instead of capacitance is necessary to account for the nonideal behaviour of the metal/solution interface [2]. Most electrochemical systems reveal such behaviour that is usually attributed to several factors, including metallurgical issues (surface roughness, presence of defects, grain boundaries, the presence of impurities, etc.), from the solution (adsorption of the compounds in solution) or of the reaction itself (formation of porous layers, corrosion products…). The impedance of this element is defined as follows[12]:

$$Z_{cpe} = A^{-1}(i\omega)^{-n}, \tag{6}$$

where A is the CPE factor, ω is the angular frequency (rad·s^{-1}), $i^2 = -1$ is the imaginary number, and n is the CPE exponent.

Table 3: Electrochemical parameters of AISI 321 in 5.5 M polluted phosphoric acid at different concentrations of AMH.

Concentration (mmol/L)	E_{corr} (mV)	$-\beta_c$ (mV)	i_{corr} (μA)	i_{pass} (μA)	i_{crit} (mA)	%IE
Blank	−376.5 ± 5.1	122.6 ± 8.7	384.1 ± 9.6	7.61 ± 1.5	1.63 ± 97 μA	—
0.5	−375.2 ± 10.5	111.4 ± 13.4	134.2 ± 12.3	9.54 ± 1.6	0.49 ± 51 μA	65.06
1	−361.6 ± 12.4	113.1 ± 11.8	101.9 ± 4.8	7.18 ± 2.3	0.21 ± 32 μA	73.48
2.5	−373.8 ± 9.7	112.8 ± 7.5	41.1 ± 4.3	6.94 ± 2.2	0.05 ± 11 μA	89.29
5	−334.8 ± 8.5	109.5 ± 10.2	17 ± 3.1	4.95 ± 1.5	0.02 ± 5 μA	95.57

To exploit the impedance analysis and explain the interface behaviour of AISI 321 in the free and inhibited solution of 5.5 M polluted phosphoric acid, an adjustment procedure was executed using an electrical equivalent circuit. From Bode diagrams, only one-time constant is distinguished across the frequency range studied in $\theta = f$ (frequency) plots. Therefore, a simple Randles circuit (Figure 9) consisting of an uncompensated solution resistance (R_s) and a constant phase element (CPE) in parallel to a faradic resistance R_F was used in our case. An excellent fitting of EIS data was found with a coefficient χ^2 of the order of 10^{-3} using the circuit mentioned below.

The impedance parameters derived from the equivalent circuit model using the EC-Lab program are presented in Table 4, and fitting curves are plotted as solid lines in the Nyquist diagrams in Figure 8(b).

The examination of the results shows that the values of inhibition efficiency become more important with the rise of AMH concentration and reaches an efficiency of 97.53% for 5 mmol/L, in agreement with the outcomes of the hydrogen evolution method (96%) and those for polarization curves (95.57%). It can be seen that as AMH concentration rises, Q_2 decreases and goes from 254.3 μF·cm^{-2} (blank) to 71.5 μF·cm^{-2} (5 mmol/L). The lowering of the double-layer pseudocapacitance may be due to the decrease of the local dielectric constant and/or the growth of the electrical double-layer thickness conforming to the expression of the double-layer capacity presented in the Helmholtz model [22]:

$$C = \varepsilon\varepsilon_0 \frac{S}{e}, \tag{7}$$

where ε_0 is the vacuum permittivity (8.8542×10^{-14} F/cm), ε is the relative dielectric constant of the layer, e is the thickness of the dielectric in m, and S is the surface area in m^2.

The adsorption of AMH on the AISI 321 surface reduces its electrical capacitance by substituting the compounds initially adsorbed on the surface (solvent molecule and other impurities present in the solution) [13, 23]. In addition, the obtained impedance plots reveal the occurrence of a single capacitive loop, meaning that the adsorption takes place by simple metallic surface coverage and that AMH acts as a primary interface inhibitor [13, 24].

3.4. Adsorption Isotherm. The corrosion inhibition of AMH mainly depends on its adsorption on the AISI 321 surface in 5.5 M polluted phosphoric acid. Therefore, adsorption isotherms are very important in describing the mode of adsorption of the inhibitor molecules on the metal surface according to their concentration. The most frequently used adsorption models are Langmuir, Freundlich, Bockris–Swinkel, Flory Huggins, Temkin, El-Awardy, and Frumkin isotherms. All these isotherms can be represented as follows [25]:

$$f(\theta, x) \exp(-2a\theta) = kC, \tag{8}$$

where $f(\theta, x)$ is the configuration factor, that is, a function of the chosen model and the assumptions established at the derivation of the isotherm. θ is the surface coverage indication, C is the inhibitor concentration in the solution, X is the size ratio, a is the molecular interaction factor, and k is the equilibrium constant of the adsorption. The previous results show that AMH inhibits the corrosion reaction by a nonreactive blockage of the AISI 321 surface. In this case, the inhibitor intervenes only by subtracting a portion of the surface from both elementary reactions, anodic and cathodic as seen in the polarization curves. Therefore, a relationship can be established between the currents involved in the absence and in the presence of the inhibitor, the surface coverage, and the inhibition efficiency.

$$\begin{aligned} i_{inh} &= (1-\theta) i_o, \\ \theta &= 1 - \frac{i_{inh}}{i_o} = \frac{E\%}{100}. \end{aligned} \tag{9}$$

Attempts to adjust the data obtained from the previous results in different adsorption isotherms reveal that the Langmuir adsorption isotherm was the most suitable to explain the adsorption behaviour of AMH on AISI 321 in 5.5 M polluted phosphoric acid. Plotting C_{inh}/θ vs. C_{inh} yielded a straight line (Figure 10) with regression coefficient (R^2) and slope being close to unity, indicating that the adsorption of AMH on the AISI 321 surface follows the Langmuir adsorption isotherm modeled by the following equation:

$$\frac{C_{inh}}{\theta} = \frac{1}{K_{ads}} + C_{inh}, \tag{10}$$

where K_{ads} is the adsorption/desorption equilibrium constant and C_{inh} is the inhibitor concentration in the solution.

The adsorbent material is often modeled by a solid substrate composed of a number of distinct sites capable of binding to the inhibitor. The adsorption process is considered as an association reaction between the inhibitor and an active site on the surface leading to an adsorbed complex (molecule-metal surface) with an associated equilibrium

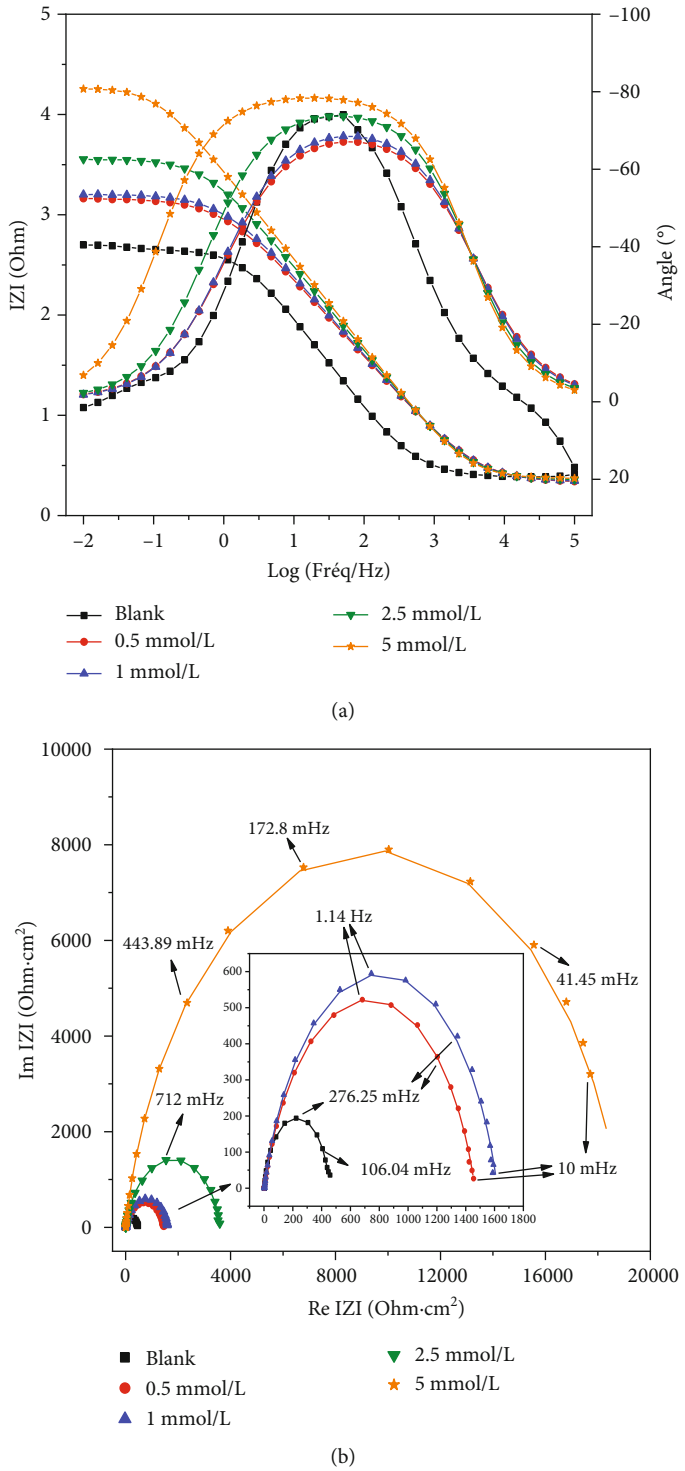

Figure 8: Bode plots (a) and Nyquist diagrams (b) for AISI 321 after 1 h of immersion at OCP potential in 5.5 M polluted phosphoric acid in the absence and in the presence of various concentrations of AMH at 20°C.

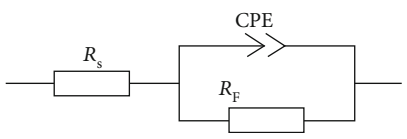

Figure 9: Equivalent electrical circuit tested for modeling of the experimental EIS (Randles circuit).

constant, K_{ads}. This association can be either electrostatic or chemical depending on the energy that combines the reagents. Based on the Langmuir model, a continuous monolayer of inhibitors surrounding the homogeneous solid surface of stainless steel and each inhibitor molecule occupy a single active anodic or cathodic site as shown by the polarization

Table 4: Impedance data of AISI 321 in 5.5 M polluted phosphoric acid with and without addition of AMH at various concentrations.

Concentration (mmol/L)	R_s (Ω·cm^2)	R_F (Ω·cm^2)	Q. 10^{-6} (Ω^{-1}·cm^{-2}·s^n)	n	χ^2 (10^{-3})	Efficiency (%)
Blank	2.45 ± 0.37	466.5 ± 0.85	254.3 ± 0.72	0.86 ± 0.5	2.85	—
0.5	2.13 ± 0.26	1453.6 ± 0.62	161.5 ± 0.4	0.79 ± 0.6	0.7	67.91
1	2.16 ± 0.18	1608.5 ± 0.43	142.1 ± 0.23	0.80 ± 0.5	3.04	71
2.5	2.26 ± 0.26	3588.1 ± 0.59	96.8 ± 0.08	0.85 ± 0.5	1.64	87
5	2.33 ± 0.23	18906.3 ± 0.74	71.5 ± 0.01	0.88 ± 0.5	9.48	97.53

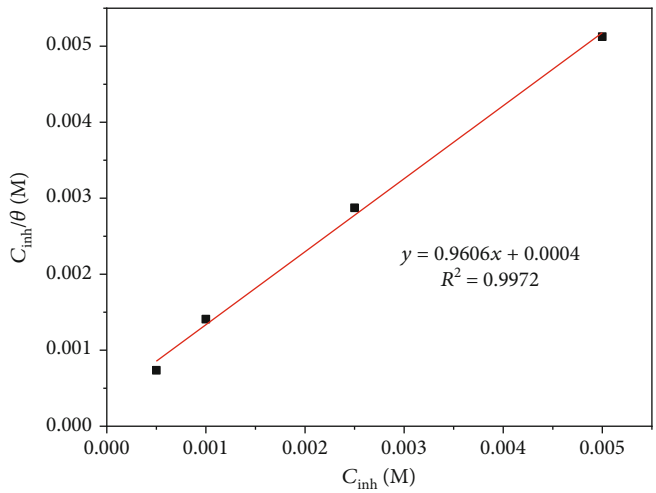

Figure 10: Langmuir adsorption isotherm of AMH on the AISI 321 surface in 5.5 M polluted phosphoric acid solution.

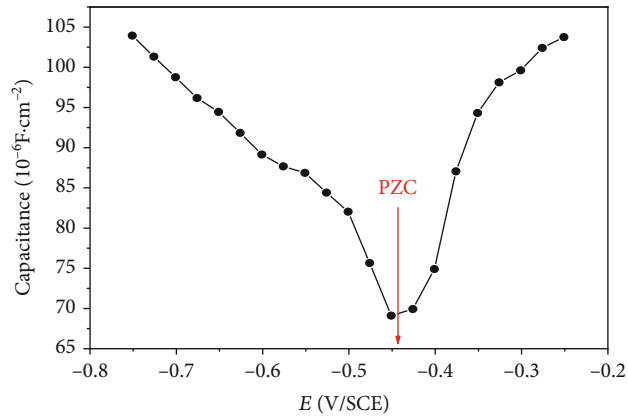

Figure 11: Evolution of polarization resistance and capacitance according to the applied potentials of alloy 321 in 5.5 M contaminated phosphoric acid with 5 mM of AMH.

curves [26]. Gibbs energy of adsorption ΔG°_{ads} can be estimated from the adsorption-desorption equilibrium constant value (K) obtained from the following relation:

$$K = \frac{1}{55.5} \exp\left(\frac{\Delta G^0}{RT}\right), \tag{11}$$

where $R = 8.314\,\mathrm{J}\cdot\mathrm{K}^{-1}\cdot\mathrm{mol}^{-1}$ is the universal gas constant, T is the absolute temperature in Kelvin (K), ΔG^0_{ads} is Gibbs free energy of adsorption, 55.5 is the concentration of water, and K_{ads} is the adsorption-desorption equilibrium constant.

The calculated free adsorption energy ΔG^0_{ads} is $-28.8\,\mathrm{KJ}\cdot\mathrm{mol}^{-1}$, which means that the adsorption of AMH on the surface of AISI 321 is a spontaneous process and reflects the stability of the adsorbed complex [27]. The calculated value of ΔG^0_{ads} lies between −20 and −40 kJ/mol suggesting a strong interaction between AMH and the surface of AISI 321, and the interaction involves both physisorption and chemisorption with a dominance of physisorption interactions [28].

3.5. Mechanism of Corrosion Inhibition. It is worth mentioning that, in acidic solutions, organic inhibitor molecules can be protonated, i.e., they can exist in their cationic form [29]. Thus, in acid solution, both neutral molecules and cationic forms of inhibitor can exist.

$$[\mathrm{AMH}] + n\,H^+ \rightleftarrows [\mathrm{AMH}H_n]^{n+}. \tag{12}$$

From previous studies, the adsorption of inhibitors depends on its total charge and the surface charge of metal. The inner potential Φ of a metal determines its surface charge; it is the difference between the free potential (E_{corr}) and the potential of zero charge (PZC) [30].

$$\Phi = E_{corr} - \mathrm{PZC}. \tag{13}$$

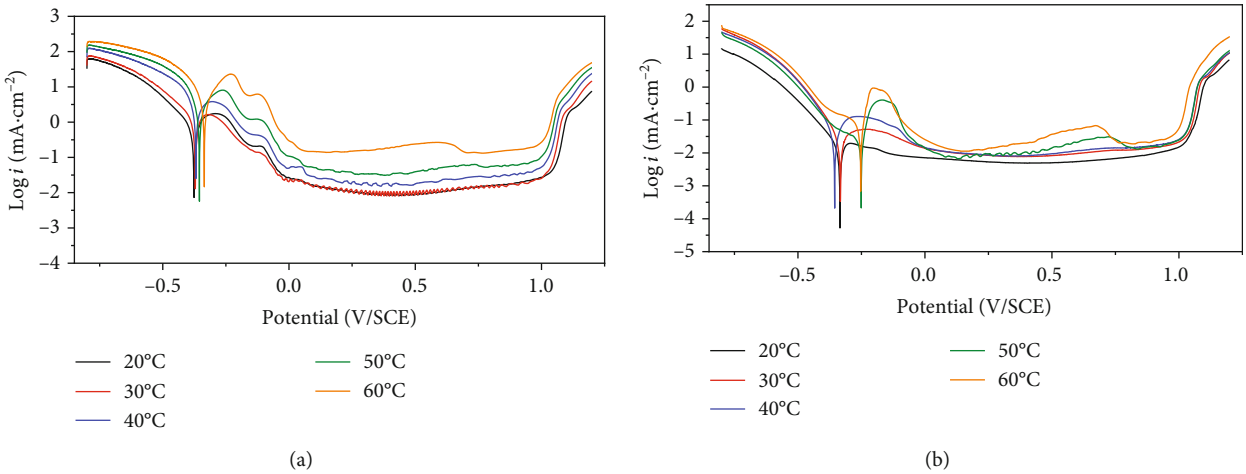

Figure 12: Effect of temperature on polarization curves of the AISI 321 corrosion rate in free (a) and inhibited (b) acid solutions.

Table 5: Various corrosion parameters for AISI 321 in 5.5 M polluted phosphoric acid in the absence and presence of optimum concentration of AMH at different temperatures.

Temperature (°C)	I_{corr} (μA/cm^2) H_3PO_4 5.5 M	5 mmol/L of inhibitor	Efficiency (%)
20	384.07	17.02	95.57
30	406.33	38.01	90.65
40	745.53	73	90.21
50	975.73	105.35	89.20
60	1671.6	173.19	89.64

The PZC is a potential that characterizes each electrochemical interface, where the solution/metal interface has no charge in the studied pH and the double layer almost no longer exists. EIS was used to evaluate the zero charge potential.

The EIS experiments were carried out by scanning the applied operating potential (anodic and cathodic potentials) excluding the OCP potential. The PZC value was obtained by measuring minimum double-layer capacitance (C_{dl}) or maximum polarization resistance (R_p) with respect to electrode potential.

Figure 11 shows the evolution of the double layer capacitance versus the applied potential for the determination of point of the zero charge potential of AISI 321 containing 5 mM AMH in 5.5 M contaminated phosphoric acid.

The plot of capacitance versus potential has a parabolic shape and the estimated PZC value is approximately −432 mV. The free corrosion potential of alloy 321 according to the OCP results was −225 mV. Therefore, the inner potential is −347 − (−432) = 85 mV, which indicates that the metal surface is positively charged in comparison to its PZC. These results suggest that the anions, the chloride, and sulfate ions will undergo an electrostatic attraction (physical adsorption) towards the positively charged metal surface and will form the primary adsorbed layer of anions on the oxide film. In our case of alloy 321, chromium and nickel exist in the passive film as (Cr_2O_3) and (NiO) [29]. After this first adsorption of anions, the electrode surface will become negatively charged; therefore, the protonated inhibitor molecules will be attached with the first adsorption layer by physical interaction.

Furthermore, AMH neutral molecules could be adsorbed on the alloy 321 surface through chemisorption mechanism, involving the displacement of water molecules from the surface and the sharing electrons through its active centers [30].

3.6. Effect of Temperature. In order to investigate the influence of elevating the medium temperature on the corrosion behaviour of AISI 321 and on the inhibiting properties of AMH, polarization curves were realized at temperatures between 20 and 60°C (Figure 12), in the absence and in the presence of 5 mmol/L of the inhibitor after one hour of immersion. The corresponding data are shown in Table 5. All the curves retain almost the same general form, with a wide passivity interval. In Figure 12(a), it's obvious that elevating acid temperature affects at the same time the cathodic and anodic reactions. The temperature rise catalyzes the reduction of protons and involves an increase of the passive current density. The transpassive potential values remain almost constant even with the harmful effect of the chloride favored by the temperature rise, as found in other studies [2]. The occurrence of a diffusion plateau at temperatures greater than or equal to 50°C in the presence of AMH suggests that the increase in cathodic current with temperature is also due to the reduction of O_2. The tests were carried out in a cell in contact with the ambient air and in the absence of agitation. It is well known that the oxygen concentration decreases with the rise in temperature. However, the diffusion coefficient of oxygen is improved with temperature, which implies a higher cathodic current density.

The corrosion inhibition efficiency of AISI 321 in 5.5 M polluted phosphoric acid using AMH decreased slightly with the temperature increment from 20 to 60°C. Desorption of AMH is favored at elevated temperatures. This shows that the inhibition occurs by an electrostatic adsorption of the inhibitor with relatively high energy, which explains the

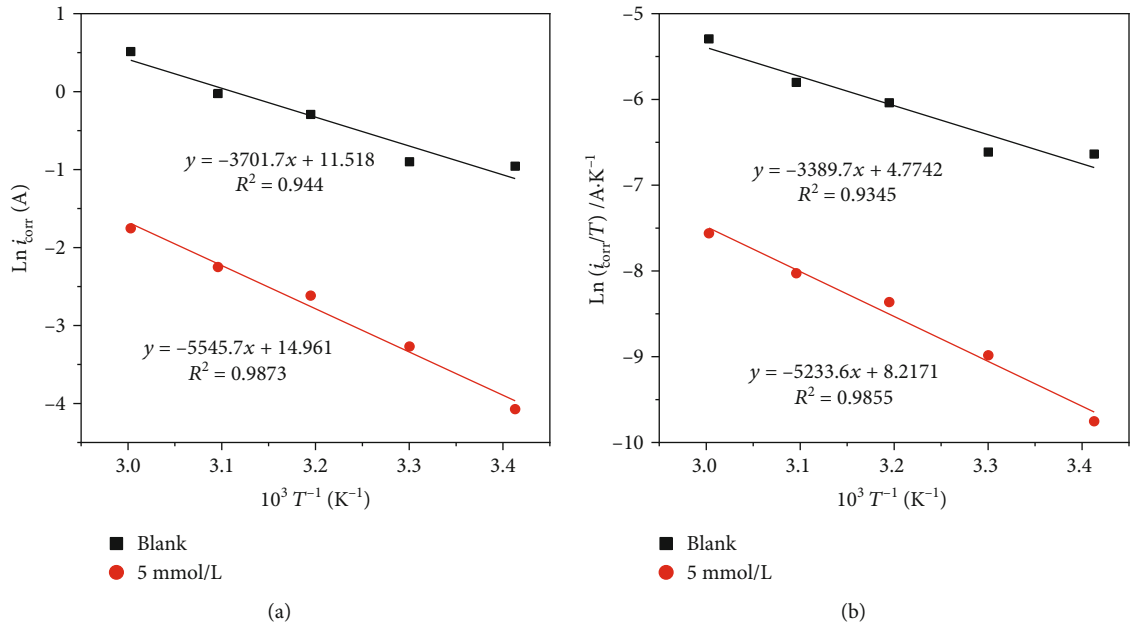

Figure 13: Arrhenius plot (a) and transition state plot (b) for the corrosion of AISI 321 in free and inhibited phosphoric acid solutions.

Table 6: Values of enthalpy of activation, entropy of activation, and activation energy of the AISI 321corrosion process in free and inhibited phosphoric acid solutions.

Inhibitor	E_a (kJ/mol)	ΔH^0_{ads} and ΔS^0_{ads} (kJ·mol^{-1})	ΔS^0_a (J·mol^{-1})
H_3PO_4 5.5 M	30.76	28.18	−215.27
$H_3PO_4$5.5 M + 5 mmol/L	46.11	43.51	−186.65

small decrease in efficiency with increasing temperature. Activation parameters of the corrosion inhibition process can be investigated using the Arrhenius equation (equation (14)) and transition state theory (equation (15)):

$$I_{corr} = A \exp\left(-\frac{E_a}{RT}\right), \quad (14)$$

$$I_{corr} = \frac{RT}{N_a h} \exp\left(\frac{\Delta S^\circ_a}{R}\right) \exp\left(-\frac{\Delta H^\circ_a}{RT}\right), \quad (15)$$

where E_a, ΔH, and ΔS are the apparent activation energy, the activation enthalpy, and entropy, respectively. A is the Arrhenius factor, R is the perfect gas constant, N_a is Avogadro's number, and h is the plank's constant.

The values of E_a were obtained using equation (14) by plotting $Ln(I_{corr})$ versus $1/T$ (Figure 13(a)), while ΔH and ΔS values were obtained using equation (15) by plotting $Ln\ (I_{corr}/T)$ versus $1/T$ (Figure 13(b)). The obtained results are summarized in Table 6.

A linear variation of $Ln \cdot I_{corr} = f\ (1/T)$ is observed, which means the implication of an active process. Activation energy is defined as the energy that requires a reagent to generate the products. The E_a values of the inhibited solution are greater than those of the uninhibited solution, indicating that the dissolution of the alloy in the presence of AMH is slow and more exigent in terms of energy [31]. This may be justified by the fact that the presence of AMH induces an additional energy for the corrosion process and that this beneficial energy rises with the increasing concentration of AMH. At higher temperatures, a noticeable decrease in the adsorption of AMH on the surface of the stainless steel is suggested and a corresponding increment in the rate of corrosion has occurred. In addition, ΔH for the inhibited solution is lower than that for the uninhibited solution with positive signs according to E_a. This fact confirms the endothermic nature of the corrosion process of AISI 321. On the other hand, entropy values have negative signs indicating a decrease in the randomness from reagents to the formed activated product. In other words, the activated compound in the rate-limiting step is obtained by an association of reagents, leading thus to more ordered elements [32].

3.7. Surface Analysis. To confirm the inhibition effect of AMH, recorded from the electrochemical experiments, on AISI 321 stainless steel, SEM images (scanning electron microscope) in the secondary electron mode were obtained from surfaces immersed in uninhibited and inhibited 5.5 M phosphoric acid solution (5.10^{-3} M) during 12 h (Figure 14). The corresponding EDX spectra are given in Figure 15.

The narrow furrow presented in the uncorroded area may be attributed to the polished trace by abrasive papers. According to the SEM image (Figure 14(a)), the surface is markedly attacked by the aggressive solution and the surface has shown a very rough morphology with numerous cavities. The addition of AMH to the corrosive medium leads to the formation of a smooth and homogeneous surface with the absence of pits compared to the blank solution. This difference is attributed to the adsorption of AMH molecules and

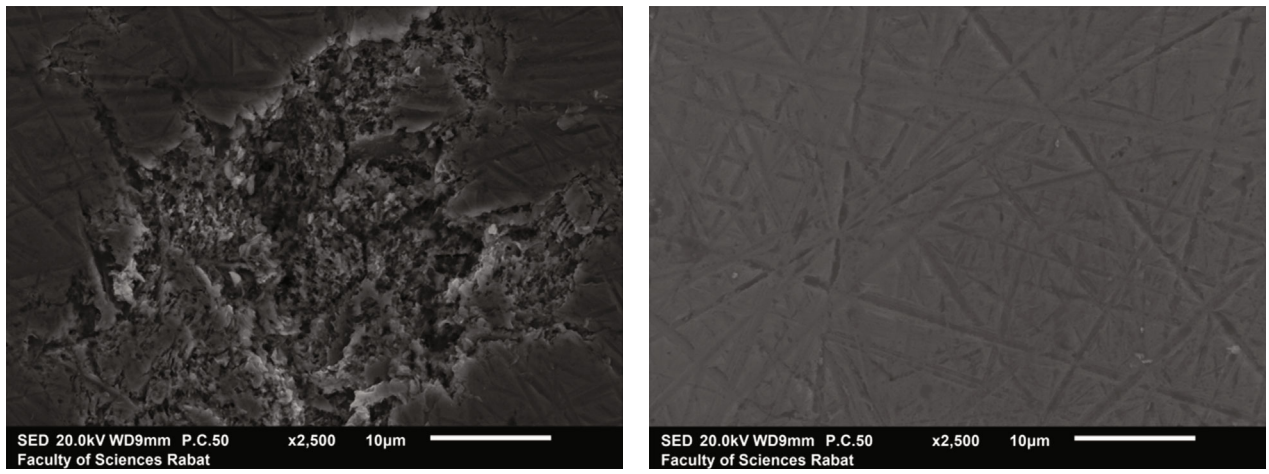

(a) (b)

Figure 14: SEM images of AISI 321 stainless steel in (a) uninhibited and (b) inhibited (with 5.10^{-3} M of AMH) 5.5 M phosphoric acid solution after 12 h of immersion.

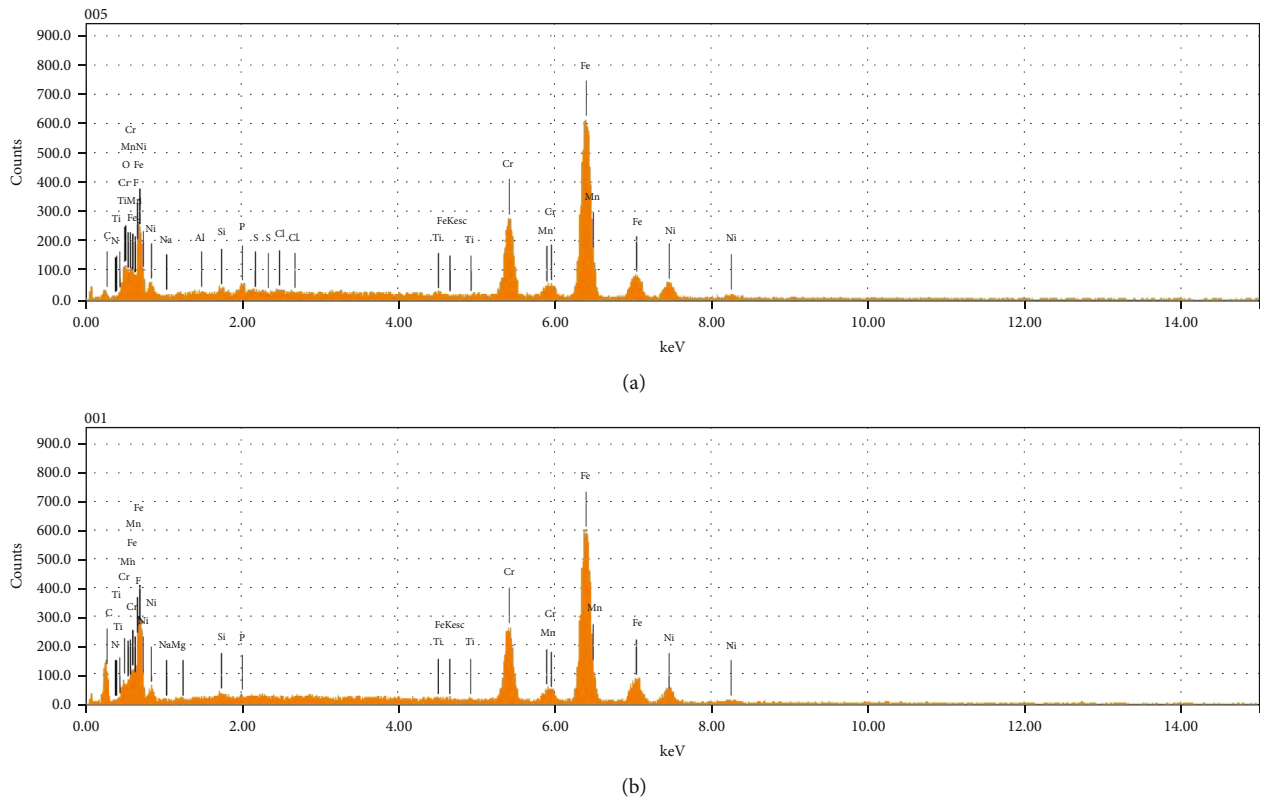

(a)

(b)

Figure 15: EDX spectra of AISI 321 stainless steel in (a) uninhibited and (b) inhibited (with 5.10^{-3} M of AMH) 5.5 M phosphoric acid solution after 12 h of immersion.

the formation of a protective layer on the surface of AISI 321 stainless steel. On the other hand, the peaks of Fe and Cl in the EDX data are attributed to general corrosion in acid medium [4]. An increase in the carbon peak of the sample is observed in the inhibited solution, which confirms the fact that AMH molecules are adsorbed on the surface of AISI 321 stainless steel and have formed a protective film.

3.8. Computational Details. Quantum chemistry methods have become a practical way for determining several molecular properties (energetic state, electronic density, geometry optimization…) and thus for correlating these properties with the various activities of molecules. In this respect, it will be possible to control the efficiency and the inhibition mechanism by linking the experimental results with those obtained

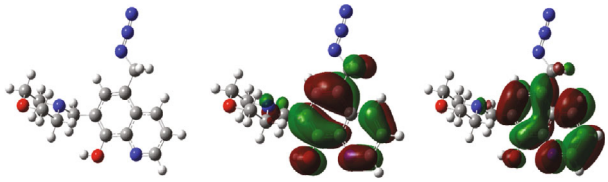

Figure 16: The frontier molecular orbital density distribution of AMH.

Table 7: Calculated quantum chemical parameters of AMH.

E (au)	−1005.68
E_{LUMO} (eV)	−1.8866
E_{HOMO} (eV)	−6.1694
ΔE (eV)	4.2828
Dipôle moment (Debye)	3.2567
η (eV)	2.1414
χ (eV)	4.028
ΔN (eV)	−0.694

theoretically [33, 34]. Figure 16 represents the optimal spatial arrangement and the patterns of the HOMO and LUMO of AMH. Generally, this graph reveals the distribution of the charge around the different types of acceptor and donor bonds depicted in the molecule in the ground and first excited states. The obtained theoretical quantum parameters are summarized in Table 7.

First, it was found that molecular energy has a negative value, which means that AMH is thermodynamically stable in aqueous solution. Investigating E_{HOMO} and E_{LUMO} is important to discover the electronic properties of molecules theoretically. The positive green phases represent a growth in the electron density, whereas the negative red phases represent a lowering in the electron density.

E_{HOMO} is usually taken as an indication of the ability of a compound to deliver electrons to a suitable substrate having an empty, low-energy orbit (metal substrate with d-vacant orbital in our case), while E_{LUMO} reflects the tendency of a molecule to accept electrons. The lower the E_{LUMO} energy of the molecule, the higher its probability of receiving the electrons [35–37]. It should be noted that compounds could undergo both electrophilic attacks and nucleophilic attacks throughout the atomic sites with a high density of the HOMO orbital and high density of the LUMO orbital, respectively [38, 39]. After the analysis of the obtained theoretical results, it was obvious that the molecule had a quasiplane structure, which allows increasing the surface covered by the inhibitor molecules using less atom excluding the multilayer adsorption way as proved by EIS tests and adsorption isotherms (high efficiency at a relatively low concentration). The value of E_{HOMO} indicates an important probability for the molecule to supply electrons to the metal with molecular free orbitals. However, E_{HOMO} has a negative sign that favors the physical adsorption of the molecule on the metal surface rather than the chemisorption [40], in agreement with the result of the adsorption energy. It is worth pointing that high-gap energy (ΔE) values imply high electronic stability and then low reactivity, while low values mean that it will be easier to remove an electron from the HOMO to the LOMO orbitals, which may result in an interesting inhibition performance [22]. The value of ΔE in our present case suggests that AMH has a strong ability to adsorb on the stainless steel surface, which corresponds to greater stability of the (AISI 321 – AMH) complex. Furthermore, the LUMO and HOMO orbitals for AMH depicted in Figure 16 are concentrated around the aromatic rings and oxygen atoms. Apparently, they are the preferred parts of the molecule that enhance its adsorption on the metal surface. On the other hand, the literature does not represent obvious correlation between the dipole moment and the inhibition behaviour. Nevertheless, most researchers admitted that inhibition efficiency should be improved with high dipole moments thanks to dipole-dipole interactions [40]. The results indicate that AMH has a high μ value, which leads to consider a possible contribution in the inhibition efficiency. The lower σ value and high value of χ imply that AMH owns an important softer nature which allows it to provide electrons and great ability to attract electrons from the metal that leads to beneficial interactions and thus higher corrosion inhibition [22]. Another important parameter that must be considered is the fraction of electron transferred (ΔN) [41]. The literature assumes that if ΔN is strictly positive, the electrons are migrated from the molecule to the substrate and if ΔN is strictly negative from the substrate to the molecule. In our case, the ΔN value is negative, suggesting a more likely transfer of electrons from the metal to AMH.

4. Conclusions

This study was dealing with the application of an ecofriendly compound, 5-azidomethyl-7-morpholinomethyl-8-hydroxyquinoline (AMH), as an inhibitor against the corrosion phenomenon for AISI 321 in 5.5 M polluted phosphoric acid. AMH acts as an excellent inhibitor for AISI 321 corrosion in 5.5 M polluted phosphoric acid solution. The inhibition efficiency of AMH is enhanced by the rise of concentration and reaches an average value of 96% for 5 mmol/L of the inhibitor based on the three used methods. The inhibition effect of AMH is explained by its adsorption on the AISI 321 surface. The adsorption process is spontaneous and follows the Langmuir adsorption isotherm. The value of ΔG^0_{ads} indicated an involvement of both physisorption and chemisorption with a dominance of physisorption interactions. Quantum chemistry calculations were conducted and have provided reasonable explanations justifying the adsorption and inhibition effect of the studied molecule. A good agreement can be observed by comparing experimental data with theoretical computation. These sets of results indicate a greater performance of AMH to prevent corrosion even at relatively low concentrations.

Data Availability

The data used to support the findings of this study are available from the corresponding author upon request.

Conflicts of Interest

The authors declare that there is no conflict of interest regarding the publication of this paper.

Acknowledgments

The authors gratefully acknowledge the help and support of the fellow scientists and colleagues that were involved in this work.

References

[1] Z. Wang, L. Zhang, Z. Zhang, and M. Lu, "Combined effect of pH and H_2S on the structure of passive film formed on type 316L stainless steel," *Applied Surface Science*, vol. 458, pp. 686–699, 2018.

[2] M. BenSalah, R. Sabot, E. Triki, L. Dhouibi, P. Refait, and M. Jeannin, "Passivity of Sanicro28 (UNS N-08028) stainless steel in polluted phosphoric acid at different temperatures studied by electrochemical impedance spectroscopy and Mott-Schottky analysis," *Corrosion Science*, vol. 86, pp. 61–70, 2014.

[3] M. G. Tsoeunyane, M. E. Makhatha, and O. A. Arotiba, "Corrosion inhibition of mild steel by poly(butylene succinate)-L-histidine extended with 1,6-diisocynatohexane polymer composite in 1 M HCl," *International Journal of Corrosion*, vol. 2019, Article ID 7406409, 12 pages, 2019.

[4] F. Bouhlal, N. Labjar, F. Abdoun et al., "Chemical and electrochemical studies of the inhibition performance of hydro- alcoholic extract of used coffee grounds (HECG) for the corrosion of C38 steel in 1M hydrochloric acid," *Egyptian Journal of Petroleum*, vol. 29, no. 1, pp. 45–52, 2020.

[5] W. Belmaghraoui, A. Mazkour, H. Harhar, M. Harir, and S. El Hajjaji, "Investigation of corrosion inhibition of C38 steel in 5.5 M H3PO4solution usingZiziphus lotusoil extract: an application model," *Anti-Corrosion Methods and Materials*, vol. 66, no. 1, pp. 121–126, 2019.

[6] S. El Hajjaji, L. Aries, J. P. Audouard, and F. Dabosi, "The influence of alloying elements on the corrosion resistance of stainless steels in phosphoric acid medium polluted by sulphide ions," *Corrosion Science*, vol. 37, no. 6, pp. 927–939, 1995.

[7] B. Erdem, A. Özcan, and A. S. Özcan, "Adsorption and solid phase extraction of 8-hydroxyquinoline from aqueous solutions by using natural bentonite," *Applied Surface Science*, vol. 256, no. 17, pp. 5422–5427, 2010.

[8] I. Garcia-Santos, J. Sanmartin, A. M. Garcia-Deibe, M. Fondo, and E. Gomez, "Structural and photophysical studies on a linear trinuclear zinc complex of 2-[(2-hydroxyethylimino)-methyl]quinolin-8-ol," *Polyhedron*, vol. 28, no. 14, pp. 3055–3059, 2009.

[9] L. E. Sarmiento, M. Rodriguez, L. Echevarria, and V. Lubes, "Speciation of the vanadium(III) complexes with 1,10-phenanthroline, 2,2′-bipyridine, and 8-hydroxyquinoline," *Journal of Solution Chemistry*, vol. 39, no. 10, pp. 1484–1491, 2010.

[10] B. Himmi, D. Douche, A. El Louzi, and K. Karrouchi, "Research article synthesis and in vitro antioxidant activity of some 8-hydoxyquinoline derivatives," *Journal of Chemical and Pharmaceutical Research*, vol. 8, no. 1, pp. 525–528, 2016.

[11] R. Y. Khaled and A. M. Abdel-Gaber, "A comparative study of corrosion inhibition of steel and stainless steel in hydrochloric acid by N,N,N′,N′-tetramethyl-p-phenylenediamine," *Protection of Metals and Physical Chemistry of Surfaces*, vol. 53, no. 5, pp. 956–960, 2017.

[12] C. Escrivà-Cerdán, E. Blasco-Tamarit, D. M. García-García, J. García-Antón, R. Akid, and J. Walton, "Effect of temperature on passive film formation of UNS N08031 Cr-Ni alloy in phosphoric acid contaminated with different aggressive anions," *Electrochimica Acta*, vol. 111, pp. 552–561, 2013.

[13] A. Mazkour, N. Labjar, E. M. Lotfi, and M. El Mahi, "Corrosion inhibition effect of 5-azidomethyl-8- hydroxyquinoline on AISI 321 stainless steel in phosphoric acid solution," *International Journal of Electrochemical Science*, vol. 16, article 210336, 2021.

[14] A. Rustandi, Nuradityatama, M. F. Rendi, and S. Setiawan, "The use of cyclic polarization method for corrosion resistance evaluation of austenitic stainless steel 304L and 316L in aqueous sodium chloride Solut," *International Journal of Mechanical Engineering and Robotics Research*, vol. 6, no. 6, pp. 512–518, 2017.

[15] F. Arjmand, L. Zhang, and J. Wang, "Effect of temperature, chloride and dissolved oxygen concentration on the open circuit and transpassive potential values of 316L stainless steel at high- temperature pressurized water," *Nuclear Engineering and Design*, vol. 322, pp. 215–226, 2017.

[16] A. Pradityana, A. S. Sulistijono, A. Shahab, L. Noerochim, and D. Susanti, "Inhibition of corrosion of carbon steel in 3.5% NaCl solution by Myrmecodia Pendans extract," *International Journal of Corrosion*, vol. 2016, Article ID 6058286, 6 pages, 2016.

[17] M. A. Amin and M. M. Ibrahim, "Corrosion and corrosion control of mild steel in concentrated H_2SO_4 solutions by a newly synthesized glycine derivative," *Corrosion Science*, vol. 53, no. 3, pp. 873–885, 2011.

[18] J. O. M. Bockris and A. K. N. Reddy, *Modern Electrochemistry, Vol. 2*, Plenum Press, New York, 1972.

[19] E. McCafferty, "Validation of corrosion rates measured by the Tafel extrapolation method," *Corrosion Science*, vol. 47, no. 12, pp. 3202–3215, 2005.

[20] Y. Obaid, A. A. Ganash, A. H. Qusti, S. A. K. Elroby, and A. A. Hermas, "Corrosion inhibition of type 430 stainless steel in an acidic solution using a synthesized tetra-pyridinium ring-containing compound," *Arabian Journal of Chemistry*, vol. 10, pp. S1276–S1283, 2017.

[21] M. Shabani-Nooshabadi and M. S. Ghandchi, "_Santolina chamaecyparissus_ extract as a natural source inhibitor for 304 stainless steel corrosion in 3.5% NaCl," *Journal of Industrial and Engineering Chemistry*, vol. 31, pp. 231–237, 2015.

[22] O. Kaczerewska, R. Leiva-Garcia, R. Akid, B. Brycki, I. Kowalczyk, and T. Pospieszny, "Effectiveness of *O*-bridged cationic gemini surfactants as corrosion inhibitors for stainless steel in 3 M HCl: experimental and theoretical studies," *Journal of Molecular Liquids*, vol. 249, pp. 1113–1124, 2018.

[23] F. E. Hajjaji, M. E. Belghiti, B. Hammouti et al., "Adsorption and corrosion inhibition effect of 2-mercaptobenzimidazole (surfactant) on a carbon steel surface in an acidic medium: experimental and Monte Carlo simulations," *Portugaliae Electrochimica Acta*, vol. 36, no. 3, pp. 197–212, 2018.

[24] N. Soltani, N. Tavakkoli, M. Khayat Kashani, M. K. Mosavizadeh, A. E. E. O. Oguzie, and M. R. Jalali, "*Silybum marianum* extract as a natural source inhibitor for 304 stainless steel corrosion in 1.0 M HCl," *Journal of Industrial and Engineering Chemistry*, vol. 20, no. 5, pp. 3217–3227, 2014.

[25] E. E. Ebenso, N. O. Eddy, and A. O. Odiongenyi, "Corrosion inhibition and adsorption properties of methocarbamol on mild steel in acidic medium," *Portugaliae Electrochimica Acta*, vol. 27, no. 1, pp. 13–22, 2009.

[26] Y. Liu, "Some consideration on the Langmuir isotherm equation," *Colloids and Surfaces A: Physicochemical and Engineering Aspects*, vol. 274, no. 1-3, pp. 34–36, 2006.

[27] A. Anejjar, R. Salghi, A. Zarrouk et al., "Investigation of inhibition by 6-bromo-3-nitroso-2-phenylimidazol[1,2-α]pyridine of the corrosion of C38 steel in 1 M HCl," *Research on Chemical Intermediates*, vol. 41, no. 2, pp. 913–925, 2015.

[28] P. Mourya, S. Banerjee, R. B. Rastogi, and M. M. Singh, "Inhibition of mild steel corrosion in hydrochloric and sulfuric acid media using a thiosemicarbazone derivative," *Industrial and Engineering Chemistry Research*, vol. 52, no. 36, pp. 12733–12747, 2013.

[29] M. Scendo and K. Staszewska-samson, "Assessment of the inhibition efficiency of 3-amino-5-methylthio-1H-1,2,4-triazole against the corrosion of mild steel in acid chloride solution," *International Journal of Electrochemical Science*, vol. 12, pp. 5668–5691, 2017.

[30] K. Satpati, M. M. Palrecha, and R. I. Sundaresan, "Electrochemical study of the mechanism of interaction of 1,2,3-benzotriazole on SS304 surface in HCl medium," *Indian Journal of Chemical Technology*, vol. 15, no. 2, pp. 163–167, 2008.

[31] T. Poornima, J. Nayak, and A. N. Shetty, "Corrosion inhibition of the annealed 18 Ni 250 grade maraging steel in 0.67 M phosphoric Acid by 3,4 dimethoxybenzaldehydethiosemicarbazone," *Chemical Sciences Journal*, vol. 3, article CSJ-69, 2012.

[32] F. O. Nwosu and M. M. Muzakir, "Thermodynamic and adsorption studies of corrosion inhibition of mild steel using lignin from siam weed (Chromolaena odorata) in acid medium," *Journal of Materials and Environmental Science*, vol. 7, no. 5, pp. 1663–1673, 2016.

[33] S. Kumar, D. G. Ladha, P. C. Jha, and N. K. Shah, "Theoretical Study of Chloro-N-(4-methoxybenzylidene)aniline Derivatives as Corrosion Inhibitors for Zinc in Hydrochloric Acid," *International Journal of Corrosion*, vol. 2013, Article ID 819643, 10 pages, 2013.

[34] G. Gece, "The use of quantum chemical methods in corrosion inhibitor studies," *Corrosion Science*, vol. 50, no. 11, pp. 2981–2992, 2008.

[35] N. Soltani, N. Tavakkoli, M. Khayatkashani, M. R. Jalali, and A. Mosavizade, "Green approach to corrosion inhibition of 304 stainless steel in hydrochloric acid solution by the extract of *Salvia officinalis* leaves," *Corrosion Science*, vol. 62, pp. 122–135, 2012.

[36] Y. Bekdemir, "Theoretical study on corrosion inhibitory action of some aromatic imines with sulphanilic acid : a DFT study," *Canadian Chemical Transactions*, vol. 3, no. 1, pp. 85–93, 2015.

[37] A. Y. Musa, W. Ahmoda, A. A. Al-Amiery, A. A. H. Kadhum, and A. B. Mohamad, "Quantum chemical calculation for the inhibitory effect of compounds," *Journal of Structural Chemistry*, vol. 54, no. 2, pp. 301–308, 2013.

[38] B. Adindu, C. Ogukwe, F. Eze, and E. Oguzie, "Exploiting the anticorrosion effects of <italic>Vernonia Amygdalina</italic> extract for protection of mild steel in acidic environments," *Journal of Electrochemical Science and Technology*, vol. 7, no. 4, pp. 251–262, 2016.

[39] S. Tripathy and S. K. Sahu, "Structural aspects and docking studies of 3-{5-[4-oxo-2-thioxo-3-(3-trifluoromethylphenyl)-thiazolidin5ylidenemethyl] furan-2-yl}-benzoic acid (OTBA) an antibacterial drug targets FtsZ protein," *International Journal of Pharmaceutical Sciences and Research (IJPSR)*, vol. 6, no. 3, pp. 1534–1539, 2016.

[40] A. Belfilali, B. Chetouani, S. L. Hammouti, S. Louhibi, A. Aouniti, and S. S. al-Deyab, "Quantum chemical study of inhibition of the corrosion of mild steel in 1 M hydrochloric acid solution by newly synthesized benzamide derivatives," *Research on Chemical Intermediates*, vol. 40, no. 3, pp. 1069–1088, 2014.

[41] R. Kumar, S. Chahal, S. Kumar et al., "Corrosion inhibition performance of chromone-3-acrylic acid derivatives for low alloy steel with theoretical modeling and experimental aspects," *Journal of Molecular Liquids*, vol. 243, pp. 439–450, 2017.